Supplementary Information: Free energy barrier and thermal-quantum behavior of sliding bilayer graphene

Jean Paul Nery,[1,2,3,*] Lorenzo Monacelli,[1] and Francesco Mauri[1,2,†]

[1] *Dipartimento di Fisica, Università di Roma La Sapienza, I-00185 Roma, Italy*
[2] *Graphene Labs, Fondazione Istituto Italiano di Tecnologia, Via Morego, I-16163 Genova, Italy*
[3] *Nanomat group, QMAT research unit, and European Theoretical Spectroscopy Facility, Université de Liège, B5a allée du 6 août, 19, B-4000 Liège, Belgium*

S1. Barrier

To determine the barrier, the free energy has to be determined at the equilibrium position and SP. At the equilibrium position, there are two shear modes, indicated with **S** in Fig. 3(b).The mode perpendicular to the bond direction shown in Fig. 1 is stable in SP, while the shear mode along the reaction coordinate (using the language of chemical reactions) is unstable. As opposed to the breathing mode, that is flat around Γ, the shear modes are only present in a small region of the BZ ($1/N^2$, with N larger than 20), as a result of the large speed of sound in graphene. So in small supercells, the shear modes will be over-represented. This is more problematic at SP, where the SSCHA frequency corresponding to she unstable mode takes very small values (see Fig. S1), which makes the convergence of the free energy hard, mostly due to the logarithm term in $F_{\mathcal{H}}$ in Eq. 4. Just determining the barrier with this equation and a $N \times N \times 1$ supercell, results in Fig. S2, which is not well converged. All SSCHA calculations used 24000 configurations, both for the barrier and the TE.

In order to get better convergence with N, we use the interpolation method mentioned in Sec. IIB, and obtain a much more stable barrier as a function of $1/N$ (see Fig. S3). The 40×40 interpolation grid used for $F_{\mathcal{H}}$ corresponds to a supercell of 6400 atoms. For 100, 200 and 300 K, the barrier seems well converged. For a 1000 K, the trend seems to indicate convergence within 0.02 meV/atom, so for the intermediate temperatures 400 and 500 K, the barrier is likely also converged within a similar error, resulting in Fig. 2 of the main text.

To better understand the reduction in the barrier, we show in Fig. S4 the SSCHA frequencies (around the shear modes) at equilibrium and SP at $T = 100$ K. The SSCHA frequencies at equilibrium are similar to the standard harmonic values, as shown in the main text. The SSCHA shear frequencies at SP instead change significantly. The shear mode that looks like an acoustic mode takes a value close to 2 cm^{-1} at Γ (see also Fig. S1). The rest of the SSCHA phonon dispersion presents small differences between equilibrium and SP frequencies.

We mentioned in the main text that in the classical limit ($\hbar\omega/kT \to 0$), the quantum distribution of the ionic displacements reduces to the classical one. We describe this here in more detail. SSCHA uses a trial harmonic Hamiltonian $\mathcal{H}$, defined in a SC, to define the density matrix $\rho_{\mathcal{H}}$ introduced in Eq. (3) of the main text. Let ω_S be the phonons frequencies and $\epsilon^S_{li\alpha}$ be the phonon eigenvectors of the interatomic force constant matrix associated to such Hamiltonian; l the index of the primitive cell within the SC, i the atomic index, α the Cartesian direction, and $S = 1, ..., 6N$ the mode (as opposed to the more common notation $\mathbf{q}s$ in reciprocal space, with $s = 1, .., 6$). It can be seen that the probability distribution of finding the crystal in a ionic configuration $\mathbf{R}$ is given by[1]

$$\rho_{\mathcal{H}}(\mathbf{R}) = A_{\mathcal{H}} \sum_{\substack{lm,ij \\ \alpha\beta,S}} \exp\left(-\frac{\sqrt{M_i M_j}\omega_S}{2n_S(T)+1} \epsilon^S_{li\alpha}\epsilon^S_{mj\beta} u_{li\alpha} u_{mj\beta} \right) \tag{S1}$$

where $u_{li\alpha}$ is the displacement from equilibrium, M_i the mass of atom i, n_S is again the Bose-Einstein factor, and $A_{\mathcal{H}}$ is just the normalization constant.

We did calculations in the classical limit by increasing the carbon atomic masses by a factor of $\tilde{M} = 600$. This reduces the phonon frequencies by $\sqrt{\tilde{M}}$, and in particular the Debye temperature below 100 K, ensuring that all modes are thermally populated. In this limit, $2n_S+1 \to 2T/\omega_S$ as we mentioned in the main text, and we can see now explicitly in Eq. (S1) that the density matrix reduces to the classical Boltzmann distribution.

Finally, we also look at the barrier in real space. That is, the difference in interlayer distance between SP and AB. Fig. S5 shows the profile of the interlayer distance, analogous to the energy profile Fig. 1 of the main text. In Fig. S6, we can see that the reduction at 100 K and temperature dependence is very similar to that of the free energy barrier, as we mentioned in the main text.

* nery.jeanpaul@gmail.com
† francesco.mauri@uniroma1.it

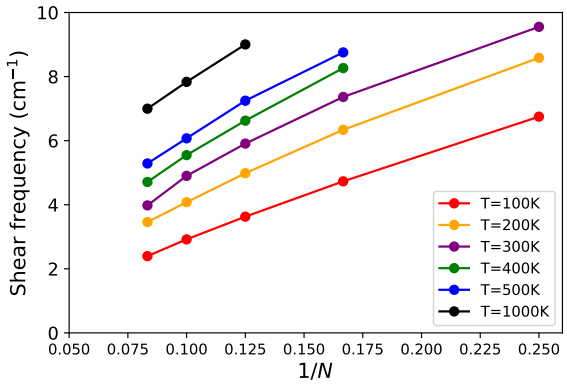

FIG. S1. Unstable shear frequency at SP as a function of $1/N$, for different temperatures. The fact that it does not stabilize shows that the shear mode is present in a small region of the BZ.

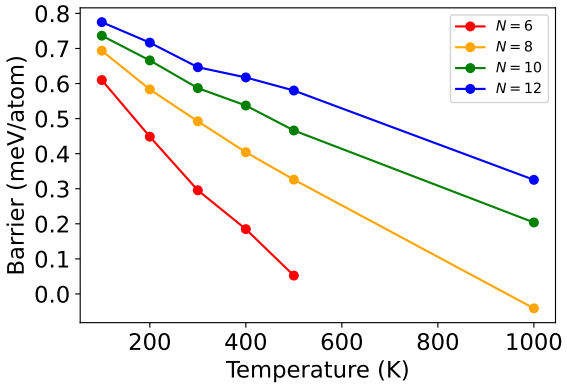

FIG. S2. Barrier as a function of temperature, for different supercells, just using the $N \times N \times 1$ grid to determine the harmonic part of the free energy Eq. (4). The barrier changes significantly with N, which means the shear mode is overrepresented. On the other hand, interpolating the harmonic part of the free energy, convergence is much better. See Fig. S3.

S2. Shear and breathing frequency

The SSCHA auxiliary and physical frequencies as a function of temperature can be observed in Fig. S7. The frequencies are not fully converged, and the converged value might be similar to the QHA. The bulk temperature dependence (corrected with the factor of the nearest neighbor model) agrees very well with QHA.

The other mode at Γ that involves the layers moving out of phase is the breathing mode (out-of-plane instead of in-plane). Its temperature dependence can be seen in Fig. S8. It decreases more at low temperatures compared to the shear mode and barrier. There are no measurements of the breathing mode as a function of temperature, so our calculations serve as a pre-

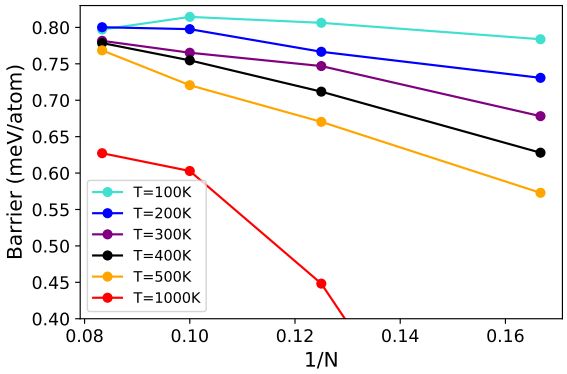

FIG. S3. Barrier as a function of $1/N$, for different temperatures, interpolating the first term of Eq. (4). The barrier seems well converged at low temperatures and harder to converge at higher temperatures. Values are likely converged within less than 0.05 meV/atom.

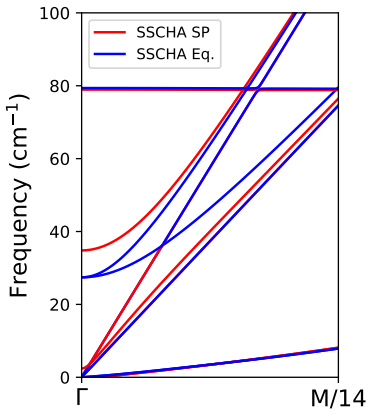

FIG. S4. SSCHA frequencies around the shear modes, at the equilibrium position (blue) and SP (red).

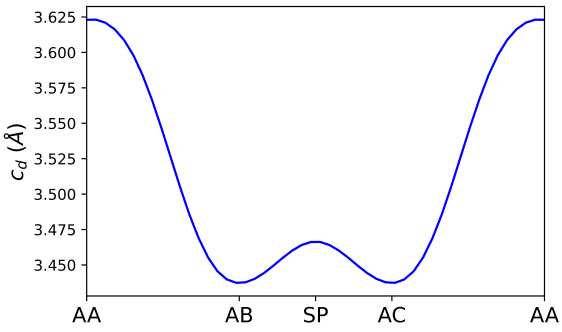

FIG. S5. Interlayer distance profile along the bond direction, when moving a graphene layer relative to another one (analogous to Fig. 1 of the main text, but for distance instead of energy). The minimum distance is at the equilibrium positions.

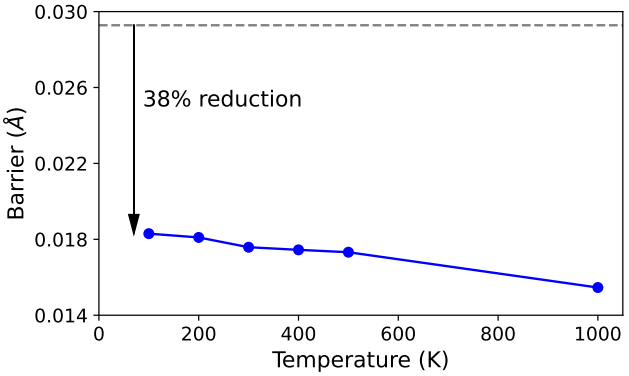

FIG. S6. Temperature dependence of the real space barrier $c_{\mathrm{SP}} - c_{\mathrm{AB}}$. It is analogous to the behavior of the free energy barrier, Fig. 2.

diction. The SSCHA curve is very well converged, so we expect it to have a temperature dependence that is closer to the experiment relative to the QHA curve. The auxiliary frequency for $N = 8$ and 10 is almost the same (Fig. S9), so the physical values are also converged (within 0.5 cm^{-1} at 1000 K, and less for lower temperatures).

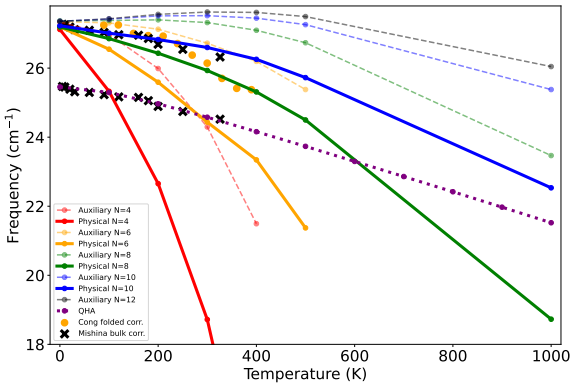

FIG. S7. Shear frequency as a function of temperature, both for the physical frequency (full lines) and the auxiliary one (dashed). The experimental value is shifted and included twice, to facilitate the comparison of the temperature dependence with the QHA and SSCHA curves. The agreement of the experimental bulk value (adjusted with the nearest neighbor model to the bilayer case) with QHA is excellent, and with SSCHA is very good as well.

S3. Thermal expansion (TE)

For the SSCHA out-of-plane TE calculations, we also used the interpolation scheme with a 40×40 grid. The interlayer distance and in-plane lattice parameter obtained in bulk with SSCHA can be seen in Fig. S10.

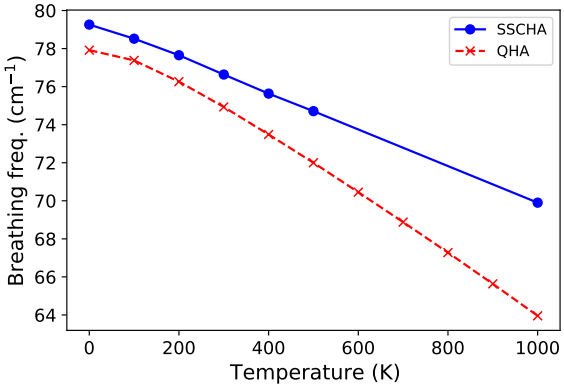

FIG. S8. Breathing frequency as a function of temperature using SSCHA (black circles) and QHA (red crosses). The SSCHA calculations are well converged and serve as a prediction, since there is no experimental data in the literature.

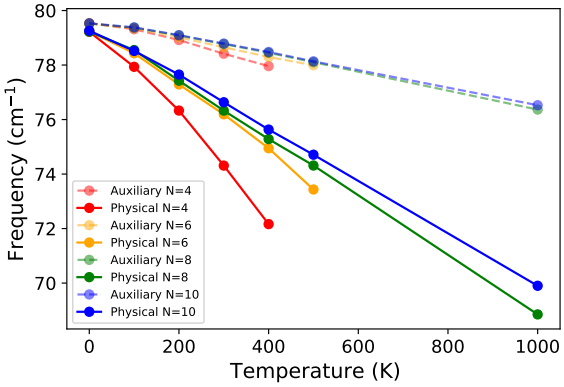

FIG. S9. Convergence of the auxiliary (dashed) and physical (full) breathing frequency. The physical frequency is well-converged at $N = 10$.

The fits are used to reduce numerical error, and correspond Eq. (6) of Ref.[2],

$$b(T) = b_0 \exp\left(\frac{X\theta}{e^{X/T} - 1}\right), \tag{S2}$$

which depends on parameters b_0, X and θ (b can be a or c_d). The derivative of the fits give the coefficients of TE. In the QHA case, the TE can be calculated quickly and accurately for many temperatures, so we just use finite differences.

In Fig. S11 we compare SSCHA and QHA for bilayer graphene and bulk. The TE for both SSCHA and QHA bulk is similarly lower relative to bilayer, and the same can be observed in Fig. 5 of Ref. 3. Since bulk values of this reference agree quite well with experiment, we expect their bilayer values to be similarly accurate, and our bilayer TE values to be similarly underestimated. In-plane, Fig. S12, we can also see a clear reduction

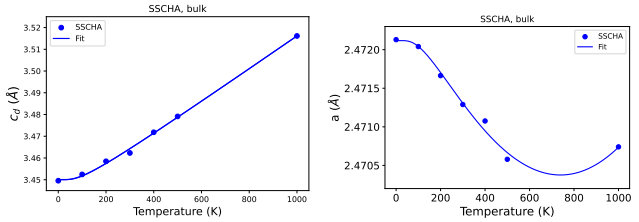

(a) (b)

FIG. S10. Out-of plane (a) and in-plane (b) SSCHA thermal expansion (blue dots). The fit corresponds to Eq. (S2).

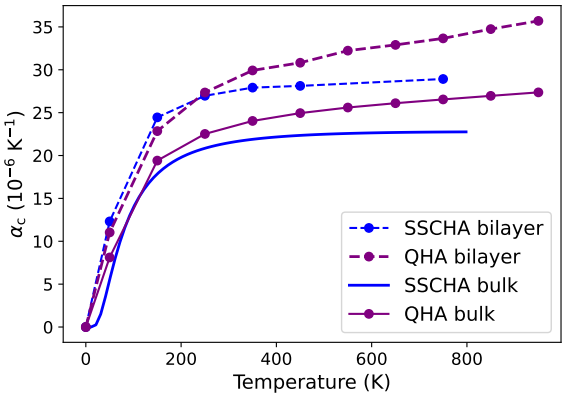

FIG. S11. SSCHA and QHA out-of-plane coefficient of TE for graphite and bilayer graphene.

of the TE coefficient from monolayer to bulk. In what follows, we describe in detail convergence studies we did for SSCHA, and also for QHA calculations.

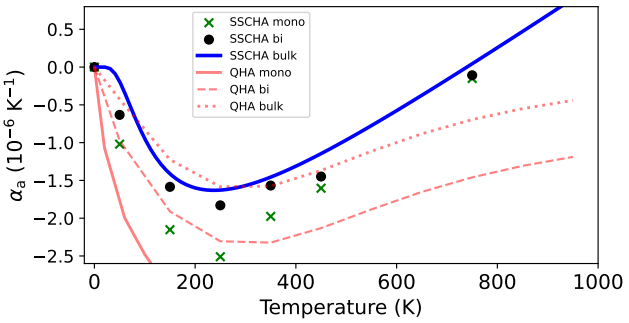

FIG. S12. In-plane coefficient of TE using SSCHA and QHA, for monolayer, bilayer and bulk.

1. *Bilayer*

QHA. We first considered the out-of-plane TE by fixing a, and then we considered the full minimization of the free energy by varying both a and c_d. In Fig. S13 we can see $c_d(T)$ both for fixed a, and for the full minimization. The full minimization has a slightly larger dependence with temperature, but fixing a is a good approximation. Fig. S14 is analogous for $a(T)$, with a fixed value $c_d = 3.5$ Å. The curves are very similar, except for a small difference at high temperatures (of about 0.0005 Å at 1000 K).

We also studied convergence with the size of the grid (Fig. S15). At $N = 12$, $c_d(T)$ is well converged (within 0.005 Å at 1000 K), although $N \sim 20$ to achieve full convergence. The shear mode increases TE because when layers are displaced relative to each other, the interlayer distance is larger (see Fig. S5). The monotonous behavior indicates that the shear modes are overrepresented for coarser grids, and become better sampled with denser grids (having wavevectors $\mathbf{q}$ closer to Γ).

In-plane, a larger N of about 50 is needed to fully achieve convergence (Fig. S16). Again, monotonous convergence suggests inadequate sampling close to Γ. Since the convergence in bulk is much faster (see below Fig. S24), we attribute the slow convergence to the flexural mode, which becomes linear (an acoustic mode) and easier to sample in bulk.

SSCHA. Out-of-plane convergence is similar to the QHA case. So $N = 12$ should give a good curve for $c_d(T)$. We also see in SSCHA a similar variation of c_d when changing a (compare Figs. S13 and S19).

On the other hand, $a(T)$ has less variation with temperature relative to QHA and is already converged at about $N = 8$ (Fig. S18).

2. *Bulk*

QHA. In bulk, there is virtually no difference for the out-of-plane TE when fixing a, or considering also the minimization of a (Fig. S20). In-plane (Fig. S21), there is a small difference between both fixing or varying a, similar to the bilayer case.

Just like in the bilayer case, relative dense grids are needed to achieve out-of-plane convergence (Fig. S22), which is again likely due to the shear mode. Regarding the extension of the supercell in the out-of-plane direction, 2 unit cells (4 layers) give good results (Fig. S23). In-plane (Fig. S24), convergence is much faster than out-of-plane.

SSCHA. Here we also used the interpolation method (40×40 grid), to go beyond the $N = 8$ supercell that was possible in the direct SSCHA calculation, resulting in the blue dots of Fig. S10 (a).

In-plane, based on $N = 8$ already giving converged results in bilayer (Fig. S18), and also considering that the QHA convergence in bulk (Fig. S24) is much faster than in bilayer (Fig. S16), $N = 8$ should give converged SSCHA results in bulk, which corresponds to the blue dots in Fig. S10 (b).

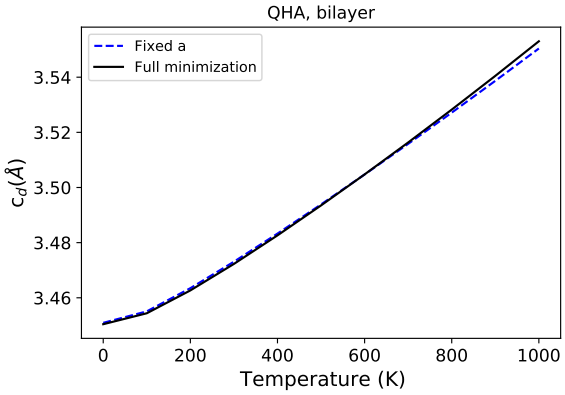

FIG. S13. Interlayer distance c_d as a functi on of temperature in bilayer graphene using QHA, fixing the value of a (dashed-blue) and doing the full minimization (full-black). In-plane TE has little effect on the out-of-plane TE.

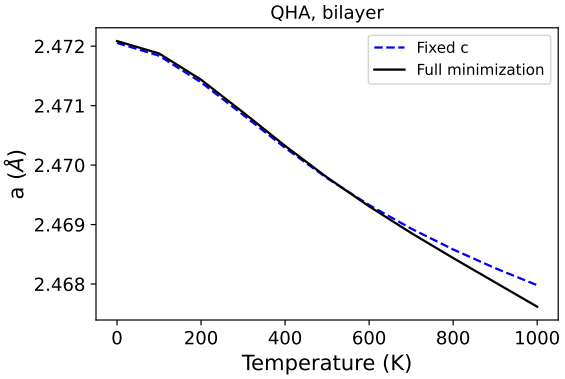

FIG. S14. Lattice parameter a as a function of temperature in bilayer graphene using QHA, fixing the value of c_d (dashed-blue) and doing the full minimization (full-black). In-plane TE has little effect on the out-of-plane TE.

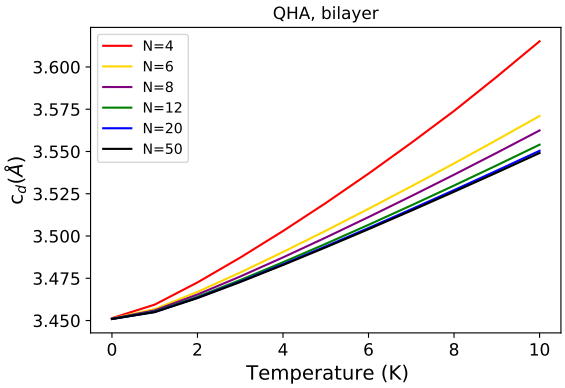

FIG. S15. Interlayer distance as a function of temperture in bilayer graphene, using QHA. At $N \sim 20$ c_d is converged, although $N = 12$ also gives a good result.

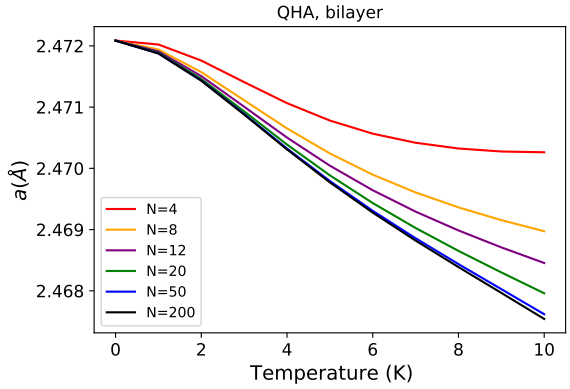

FIG. S16. In-plane lattice parameter as a function of temperature in bilayer graphene for different N using QHA. A large N is needed to achieve convergence.

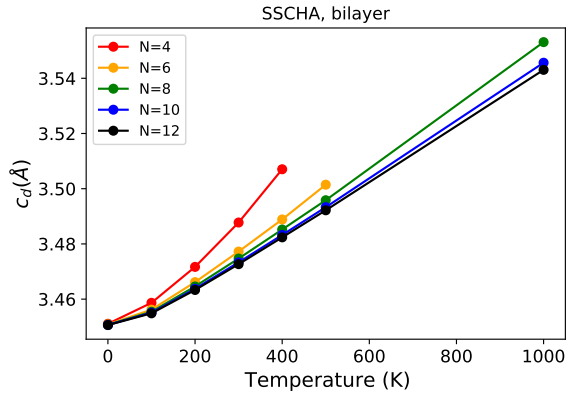

FIG. S17. Interlayer distance as a function of temperature in bilayer graphene for different N using SSCHA. Convergence is similar to the QHA case, Fig. S15, where $N = 12$ gives a good value of $c_d(T)$.

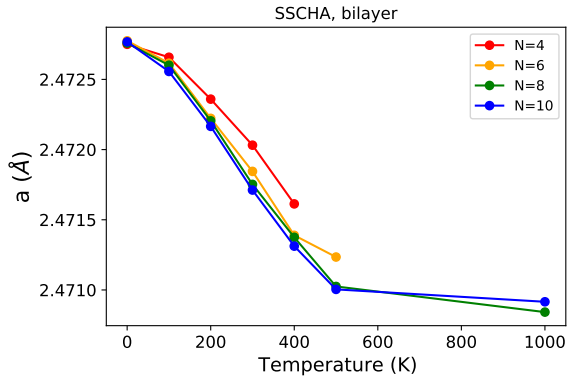

FIG. S18. In-plane lattice parameter as a function of temperature, for different N. At $N = 8$ the curve is already well converged.

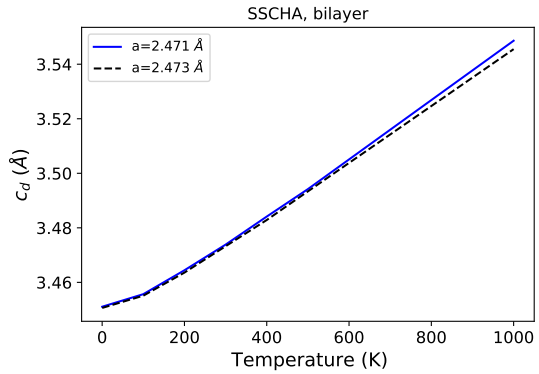

FIG. S19. Interlayer distance as a function of temperature in bilayer graphene, using SSCHA, at two different values of the in-plane lattice parameter. The curves are similar to the ones of Fig. S13. In-plane TE has little effect on the out-of-plane TE.

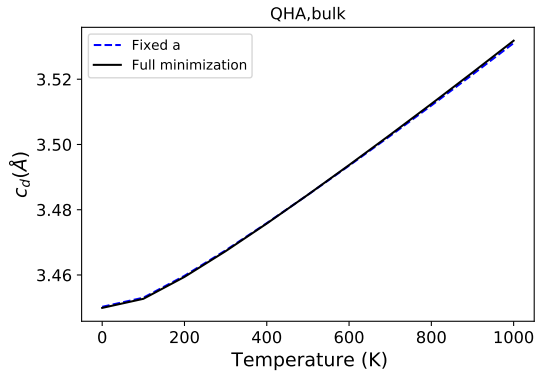

FIG. S20. Interlayer distance as a function of temperature in bulk using QHA, fixing the value of c_d (dashed-blue) and doing the full minimization (full-black). In-plane TE has barely no effect on the out-of-plane TE.

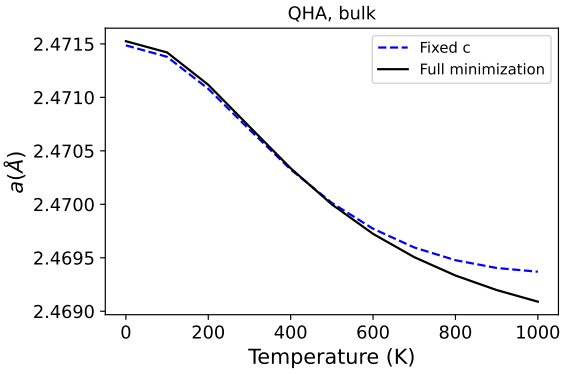

FIG. S21. In-plane lattice parameter as a function of temperature in bulk using QHA, fixing the value of c_d (dashed-blue) and doing the full minimization (full-black). The out-of-plane TE has a slightly larger but similar effect relative to bilayer on the in-plane TE.

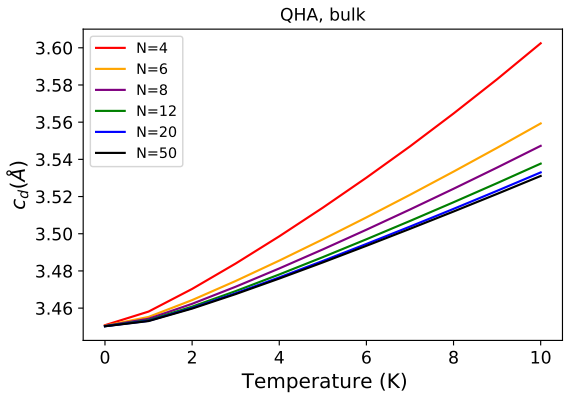

FIG. S22. Interlayer distance as a function of temperature in graphite for different N using QHA. Convergence is similar to the bilayer case.

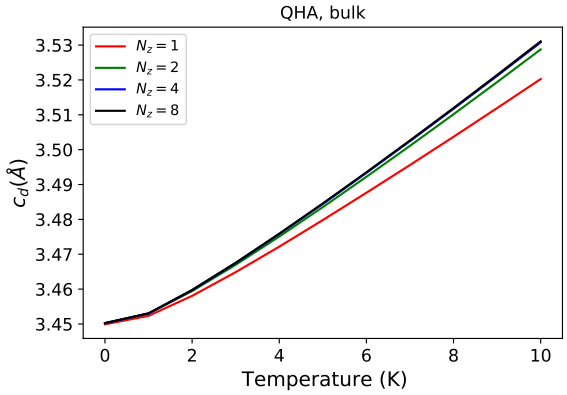

FIG. S23. Interlayer distance as a function of temperature in graphite for different N_z. $N_z = 2$ is the value used in our calculations.

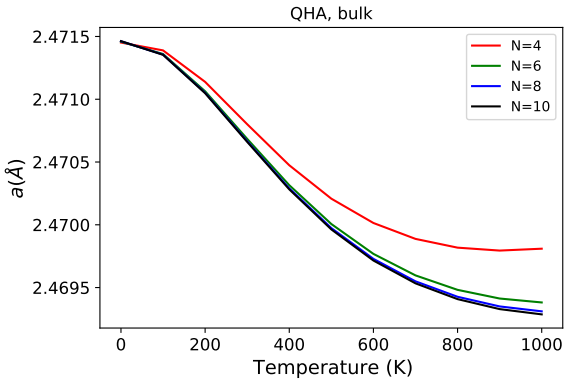

FIG. S24. In-plane lattice parameter as a function of temperature in graphite using QHA, for different N. At $N = 6$ convergence is already very good, as opposed to the bilayer case Fig. S17.

[1] I. Errea, M. Calandra, and F. Mauri, Anharmonic free energies and phonon dispersions from the stochastic self-consistent harmonic approximation: Application to platinum and palladium hydrides, Physical Review B **89**, 064302 (2014).
[2] J. E. Zorzi and C. A. Perottoni, Thermal expansion of graphite revisited, Computational Materials Science **199**, 110719 (2021).
[3] C. P. Herrero and R. Ramírez, Thermodynamic properties of graphene bilayers, Physical Review B **101**, 035405 (2020).